NIKA2-Pol : summary of polarization commissioning report

NIKA2-Pol commissioning team (H. Ajeddig, Ph. André, F.-X. Desert, S. Leclercq, J.F. Macias-Perez, A. Maury, I. Myserlis, N. Ponthieu, A. Ritacco)

January 26, 2024 - v3

Main findings

- Our observations suggest that the polarization angles obtained through the system {30m+NIKA2} are stable over the probed ~ 2 years timescale (dispersion $\lesssim 5°$)
- According to the commission analysis an offset of $\sim -5.6° \pm 1°$ might have to accounted for, and is implemented in the current PIIC software available to IRAM users.
- NEFDs are shown to be consistent over two years up to a 10% uncertainty on absolute calibration. The NEFD on total intensity, $\sim 33\,\mathrm{mJy.s}^{1/2}$ is close to that obtained in total power mode and reported in Perotto et al (2020) (at 24 Hz and without the HWP in the optical path). Sensitivity in polarization is better than in total power, with values close to $20\,\mathrm{mJy.s}^{1/2}$ in Q and U.
- Without any correction, NIKA2-POL data can be affected by instrumental polarization (IP) at a level of up to $\pm 3\%$, especially in the case of compact sources. At this stage, IP correction cannot be guaranteed in the software supported for the NIKA2 users. However, observations of strong unpolarized point sources may allow to monitor the polarized beam and mitigate the IP. Thus, for projects using NIKA2 polarization capabilities we recommend to include regular observations of a bright unpolarized point source close to the target source(s), and consider the extra overheads accordingly.

NIKA2 (New Instrument of Kids Array, see Adam et al. 2018; Perotto et al. 2020) is the dual-band wide-field continuum camera which is installed since October 2015 in the cabin of the IRAM 30 m telescope (Pico-Veleta, Spain). This camera hosts three arrays of frequency multiplexed LEKIDs (Lumped Element Kinetic Inductance Detectors) cooled at 100 mK. The signal from the two 1140-pixels arrays operating at 1.15 mm can be used to recover the polarized light from astrophysical sources: the modulation of the incoming wave by a continuously rotating half-wave plate and its combination to a polariser allows to select the polarization state and therefore measure the linear polarization of the 1.15mm continuum emission. The polarization hardware and data acquisition system are described in Ritacco (2016).

Three NIKA2 polarization commissioning campaigns were carried out: a first campaign in December 2018, a second campaign in February 2020, and a third campaign in November 2020. These campaigns aimed at assessing the stability, accuracy, and sensitivity of the polarization system on NIKA2. How these goals were addressed and the test observations that were carried out in these aims, in each of these campaigns, will be detailed in a forthcoming paper by the commissioning team, in preparation. This commissioning report provides a summarized overview of results with the goal to inform IRAM users in the scope of the opening of the polarimetric capabilities of NIKA2 to the IRAM community.

1 Summary of the polarization pipeline used for commissioning campaigns

We provide here a summary of the data processing that is specifically involved in the reduction of NIKA2 polarized data. A publication, in preparation, will provide more details on the polarization data and the pipeline processing implemented.

Data are processed on a scan by scan basis, before they are combined in a final map when several scans of the same object are available. We here summarize the overall data processing specific.

For each scan:

1. Read the raw data from the instrument and the antennaIMBifts

2. Perform all the low level processing on KID timestreams, a.k.a. time-ordered information (TOI) as in the standard pipeline presented in Perotto et al (2020) and the total power commissioning report : deglitching, opacity correction, calibration etc.

3. Subtract the Half Wave Plate Synchronous Signal (HWPSS), while masking bright sources. In the case of bright diffuse emissions, this might need iterations, like for diffuse emission map-making and baselines or "common modes" estimation-subtraction

4. Perform the lockin operation : multiply by $\cos 4\omega$ and $\sin 4\omega$ and lowpass to obtain 2 timelines per KIDs, one of pure Q, one of pure U. The pure I timeline is obtained by a simple lowpass.

5. Deal with the pure I timelines as for standard NIKA2 observations (sky noise and electronic noise decorrelation etc.). For Q and U timelines, there is negligible low frequency residuals.

6. Project these timelines onto three separate maps of I, Q and U.

2 Characterizing the instrumental polarization (IP) pattern

From a detailed analysis of the IP pattern and IP level observed for Uranus observations during the commissioning campaigns, our main conclusions are:
(1) Under good observing conditions and for well-focused data, the IP or leakage pattern takes the form of a characteristic "cloverleaf" structure, with a central positive spot surrounded by a negative quadrupole, in both Stokes Q and (a lesser extent) Stokes U (see, e.g., Fig. 1).
(2) On short timescales, the IP pattern is invariant in Nasmyth coordinates. It slowly rotates with elevation in horizontal coordinates (and more quickly rotates with parallactic angle in equatorial coordinates). On longer timescales, the orientation of the pattern also exhibits weaker changes in Nasmyth coordinates, an effect which appears to be related to the telescope astigmatism

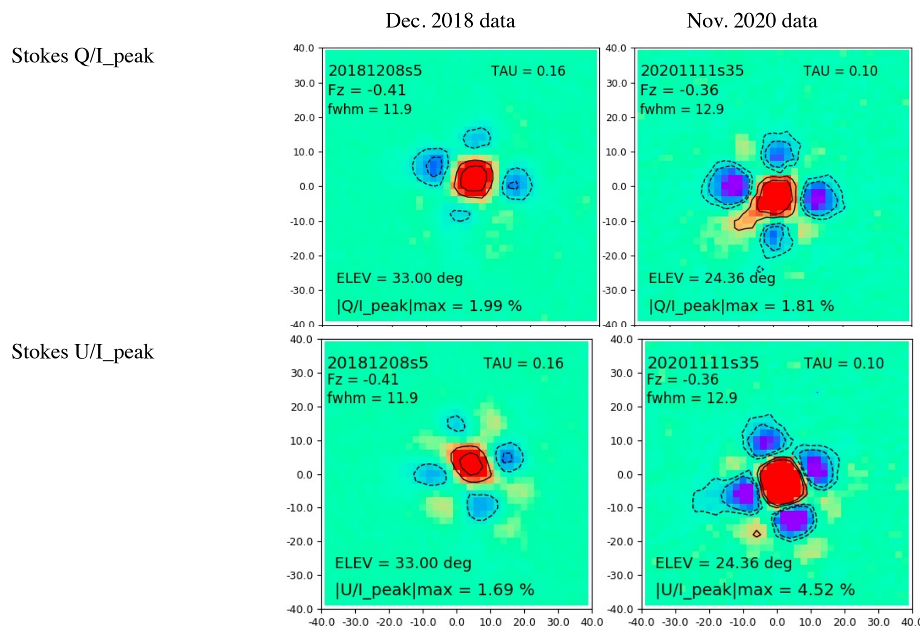

Figure 1: Examples of Stokes (Q, U) leakage maps (in Nasmyth coordinates) obtained on Uranus during the Dec. 2018 (left column) and Nov. 2020 (right column) runs. Uranus being an unpolarized calibrator, theses maps provide the pattern of NIKA2-POL instrumental polarization. Note the cloverleaf shape. The leakage pattern in both Stokes Q and Stokes U is stable from day to day under similar observing conditions.

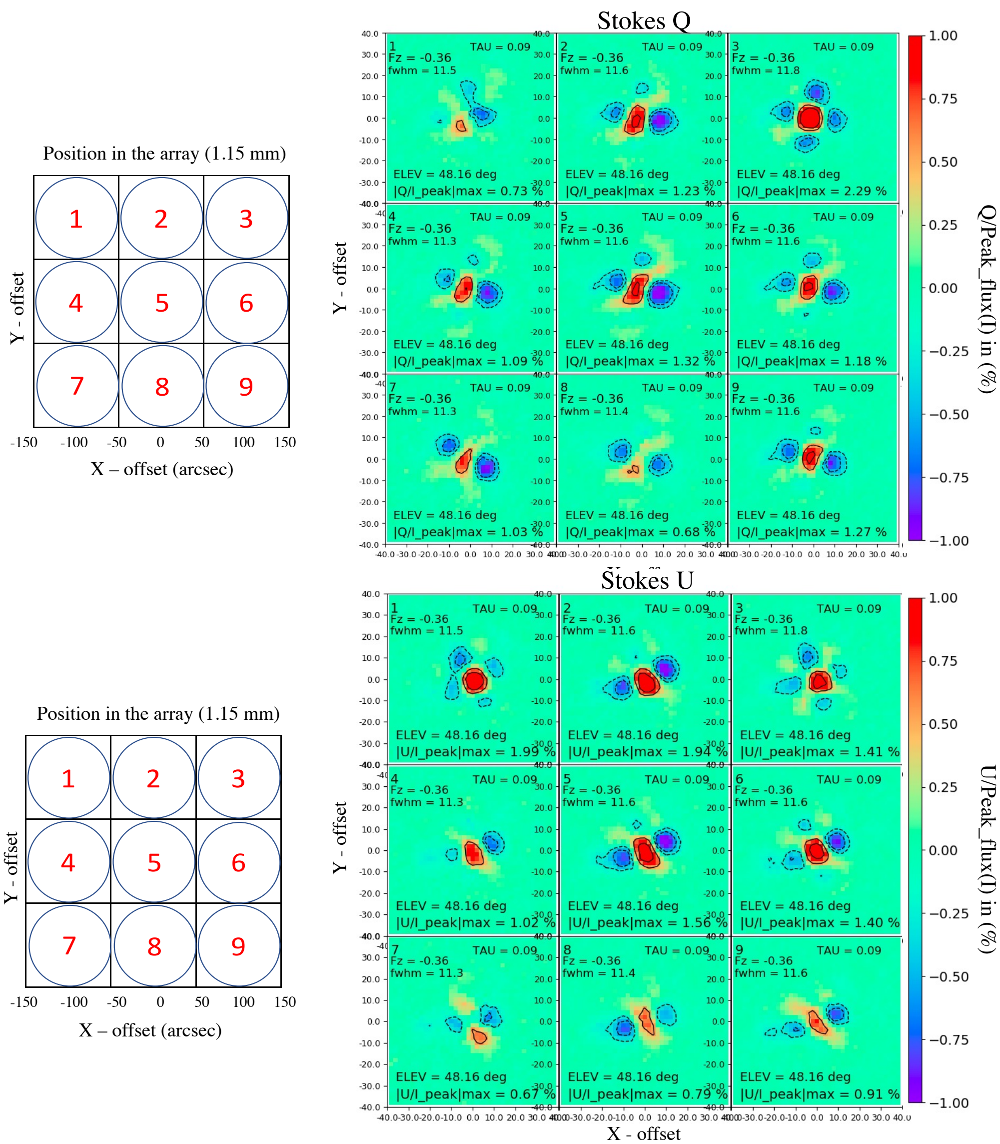

Figure 2: Variation of the IP pattern/intensity as a function of position in the NIKA2 field of view (FoV), combining Array 1 and 3. Offsets are in Nasmyth coordinates. **Left** : Location in the FoV marked by numbers from 1 to 9, with 5 representing the central region of the FoV. The diameter of each circle is 100 arcsec. **Right** : Leakage pattern in Stokes Q and U for each of the 9 regions of the FoV schematically shown on the left.

(3) The IP level and pattern are quite sensitive to the focus position of the telescope, with a focus offset of $\pm$ 0.2 mm leading to a significantly different IP.
(4) The level of IP varies with elevation and shows a different pattern at elevations $< 30°$.
(5) The IP pattern has only weak variations depending on position in the field of view of the KIDS array(s) (see Fig. 2).
(6) The IP pattern is not strictly identical but very similar for Array 1 and Array 3 (see Fig. 3).
(7) Under similar observing conditions (in terms of elevation, focus, atmospheric opacity), the IP presents both a similar pattern and a similar level.

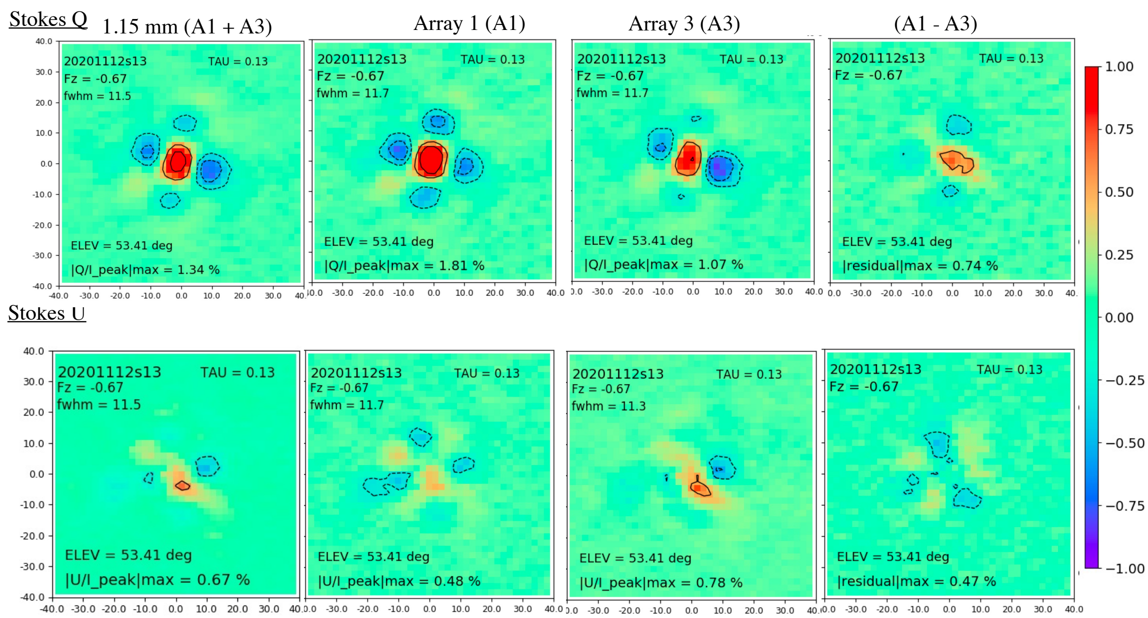

Figure 3: Comparison of the leakage patterns affecting Array 1 and Array 3, based on observations of Uranus. From left to right, leakage pattern for the combination of A1 and A3 data, for A1 data only, for A3 data only, and difference between the A1 and the A3 pattern. The leakage patterns are quite similar in A1 and A3, but the IP level seems to be slightly higher in A1 than A3 (e.g. 1.81% versus 1.07% in Stokes Q here, for this particular scan of Uranus). In both Stokes Q and U, the difference between the A1 and A3 patterns is $< 0.75\%$.

Without correction, the typical {NIKA2-Pol+30m} instrumental polarization observed in the commissioning data can be up to a few percents. Because the amplitude of the leakage pattern is mostly contributing to add spurious signal at small scales, the leakage effect is relatively important in compact sources with strong Stokes I, such as quasars. For compact, weakly-polarized sources, leakage correction could be carried out only when a strong, compact unpolarized source is observed nearby (as an example, Uranus was used for the commissioning campaigns).

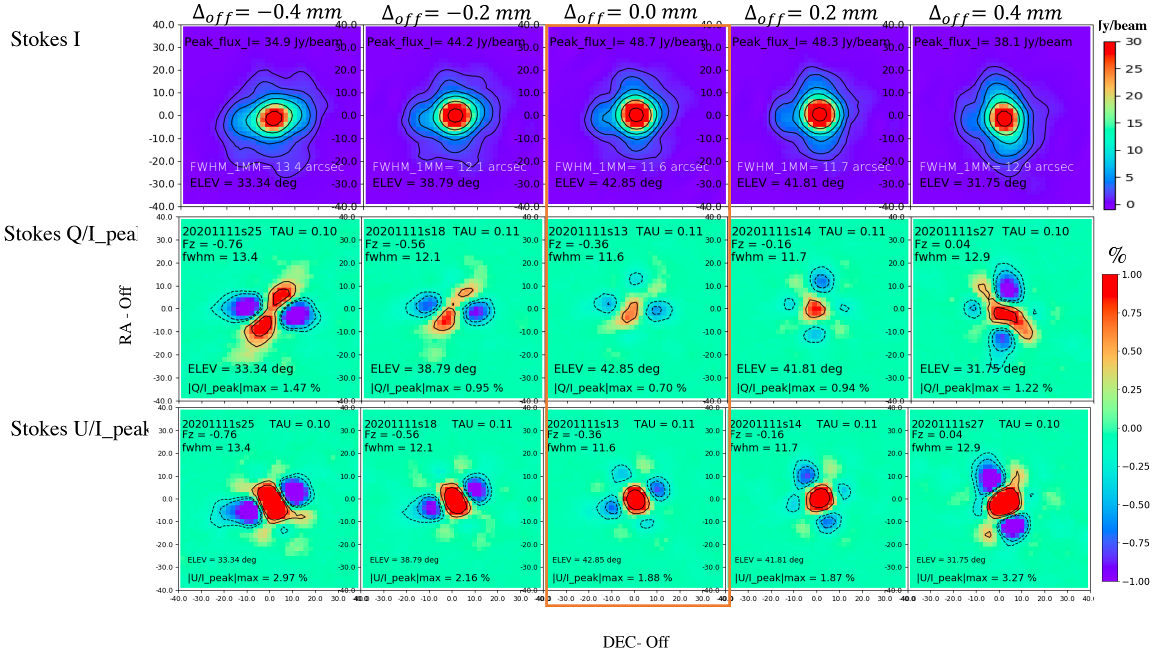

Figure 4: Example of a focus sequence on Uranus in Nasmyth coordinates showing how the instrumental polarization pattern (Stokes Q and U emission maps from an unpolarized source) varies as a function of the offset from the optimum focus position (along the Z-axis). The typical cloverleaf pattern seen at the best focus position becomes more severely distorted as the applied focus correction is farther away from its optimum value. The central map here is the one taken at a good focus position and the correction is named by Δ_{off} for positive and negative corrections with respect to the optimum leakage pattern from the left and to the right panel, respectively.

3 Polarization angles: stability over time and absolute angle calibration

Using the results from 3C286, OMC-1 and the Crab nebula we could conclude that the absolute angle calibration on the sky of $-5.6^\circ \pm 1^\circ$ seems constant across time and source properties. The origin of this angle offset is yet undetermined (it could come from e.g. an angle in one of the optical elements, from an uneven incidence on the dichroic, or even from a small angle between the HWP extraordinary axis and the splitting grid transmission axis), but its constant nature makes it easily corrected to calibrate the NIKA2-Pol measurements and reproduce well-known polarization angles from the literature. Our analysis also demonstrates a very good stability of the measured polarization angles over the three campaigns in these sources, spanning over two years. The NIKA2-Pol results in 3C286, OMC-1 and the Crab hence show that, although the origin of this constant angle offset is not yet fully understood, we can satisfactorily correct the NIKA2-Pol measurements to obtain robust and repeatable polarization measurements in astrophysical sources.

4 Sensitivity estimates

4.1 Method

Observations of sources in the three campaigns were also used to derive Noise Equivalent Flux Density (NEFD) values in both total power (Stokes I) and polarization (Stokes Q and Sokes U). The NEFD for each Stokes parameter is estimated either by scan and extrapolated to top-of-atmosphere conditions, or by checking and fitting the noise decrease as a function of increasing effective integration time. We remind that this effective integration time is derived from the number of samples projected on the map at the center, the density of KIDs per beam and is extrapolated to outside the atmosphere so that the NEFD can be directly fitted as the amplitude of the 1/sqrt(time) fitting curve (see Perotto et al, 2020 section 10.1 for an extensive discussion). This explains why the effective integration time is not the same at 1 and 2mm in Figure 5.

Fields containing faint (< 0.1Jy in both Stokes I, Q and U) and rather compact sources are the best candidates to follow the evolution of noise with integration time, we have computed independent NEFDs from each of the sources observed the most in depth during each of the three campaigns: CX-Tau, 3C286 and B335.

4.2 Results

We show in Figure 5 the decrease of the sensitivity on the estimate of CX-Tau flux as observed in campaign # 1. Table 1 reports all the NEFDs values found for the different sources that were observed over long integration times, for the three campaigns.

Considering an absolute flux calibration error of the order of 10%, which is standard for NIKA2, and in general for mm ground facilities, these NEFDs values are consistent with each other and stable in time. Note that, at the time of the writing of this document, absolute flux calibration consistency between NIKA2 campaigns spanning over several years was still subject to uncertainties: combining data from all 3 campaigns does not improve the accuracy of those measurements. The NIKA2-Pol NEFD in I, Q and U are better than the specifications: they are shown in the Table below.

Note that the sensitivity in Q and U is paradoxically better than the no-polar I sensitivity. For white noise, we would expect Q and U sensitivity worse by $\sqrt{2}$ than in I. In the NIKA2 case, it is better by 1.5. This is understood as a benefit from the fast modulation of the polarization by the HWP that puts the signal around 12 Hz, far from atmosphere and electronic noise residuals. Indeed, the lockin detection happens at 4 times the HWP rotation frequency, that is to say 12 Hz where the instrumental noise is mostly white and atmosphere drastically reduced. Hence Q and U show excellent sensitivities.

References

Adam, R., Adane, A., Ade, P. A. R., et al. 2018, , 609, A115

Perotto, L., Ponthieu, N., Macías-Pérez, J. F., et al. 2020, , 637, A71

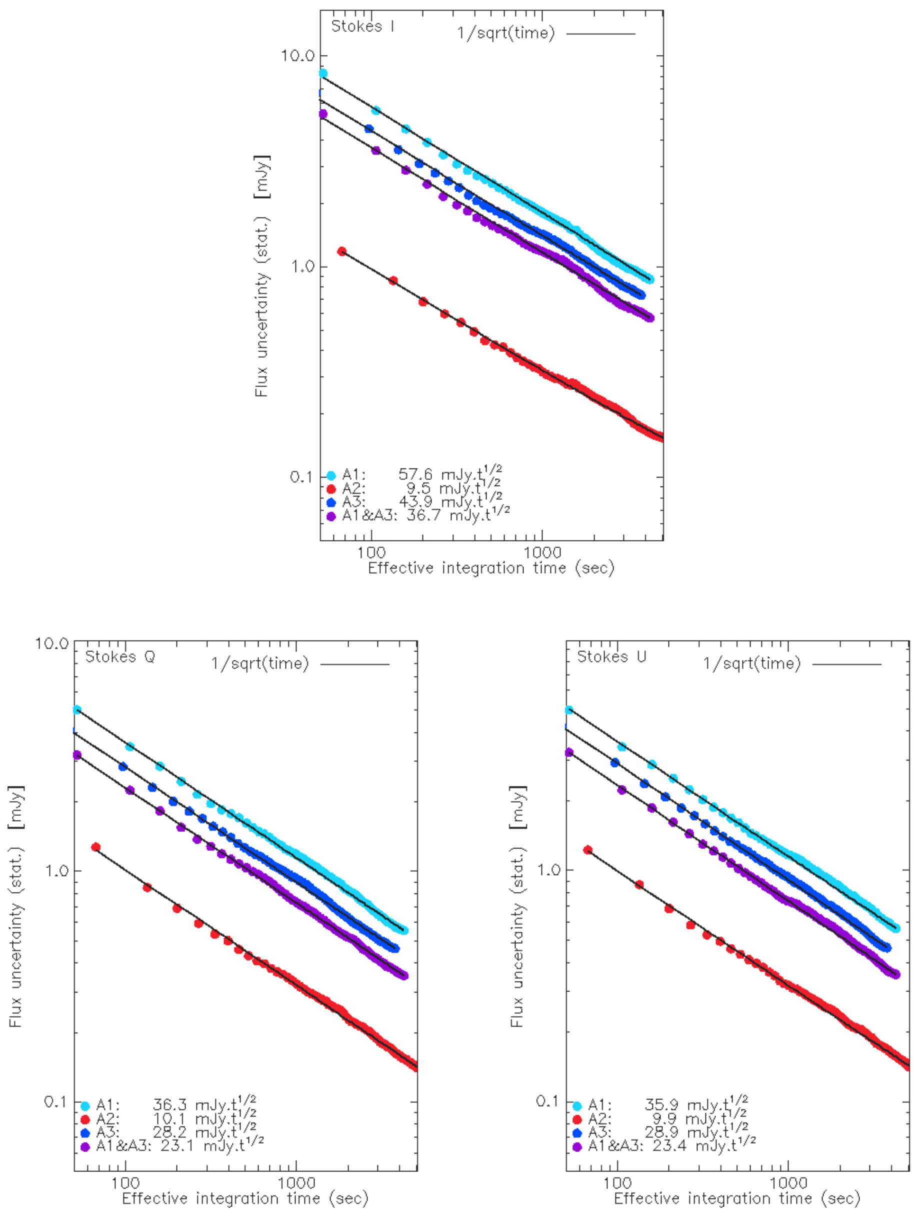

Figure 5: Decrease of the sensitivity on the estimate of a point source flux (CXTau in campaign #1) in I, Q and U as a function of the integration time per beam.

Ritacco, A. 2016, Theses, Laboratoire de Physique Subatomique et de Cosmologie ; Université Grenoble - Alpes

Table 1: Estimated NIKA2 NEFD values in each campaign and for each Stokes parameter in mJy.s$^{1/2}$. The integration time reported in this table is the time spent at the center of the map, on source, on a single beam scale, corrected for opacity (see text and Perotto et al (2020) for an extended discussion on this definition).

Campaign: Source	Combined 1mm			Integration time (s)
	I	Q	U	
#1: CX-Tau	37	23	23	4262
#1: 3C286	35	23	24	5659
#2: 3C286	34	20	20	2844
#2: 3C279	36	20	20	997
#3: 3C286	29	19	19	2432
#3: B335	29	19	20	1566